ORIGINAL RESEARCH

Differential Diagnosis of Intracranial Malignant Tumors Using MRI Based on Morphological Features and Signal Intensity Ratio of Lesions

Hongmei Yu, MM; Min Chen, MM; Yi Huang, BM; Peng Wang, MM; Jianhao Li, MM; Qing Li, BM; Rui Jiang, MM

ABSTRACT

Objective • To investigate the clinical value of conventional MRI morphological features and signal intensity ratio in the differential diagnosis of intracranial malignant tumors (high-grade glioma (HGG), primary central nervous system Lymphoma (PCNSL) and single brain metastasis (BM).

Methods • Retrospective analysis of 92 cases of HGG, 27 cases of PCNSL, and 35 cases of BM. MRI data in The General Hospital of Western Theater Command from August 2014 to December 2021, comparative analysis of morphological characteristics of tumors and lesion/normal brain parenchyma signal ratio (lesiontonormal parenchymaratio, LNR), five indexes were included T_1WI signal ratio (LNRT1), T_2WI signal intensity ratio (LNRT2), T_2WI/T_1WI signal ratio (LNRT2/T1), T_1WI enhanced signal ratio (LNRT1CE) and contrast enhancement ratio (CER). The differential diagnostic performance was also assessed by subject operating characteristic (ROC) curves.

Results • HGG, PCNSL, and BM were all seen more frequently in the supratentorial region, More than 50% of HGG mainly showed irregular morphology, intratumoral necrosis, cystic degeneration, peritumoral severe edema, cyclic uneven enhancement after enhancement, PCNSL significantly enhanced the main uniformity, necrosis cyst became rare, BM group showed uneven enhancement, no obvious specificity, and the differences in tumor morphology, peritumor edema, intratumor hemorrhage, necrotic cystic lesions, and enhancement patterns were statistically significant among the three ($P < .05$). PCNSL LNRT1 and its LNRT1CE (LNRT1: 0.558 ± 0.050, LNRT1CE: 1.637 ± 0.125) were significantly higher than those of HGG (LNRT1: 0.480 ± 0.077, LNRT1CE: 1.425 ± 0.160) and BM (LNRT1: 0.514 ± 0.120, LNRT1CE: 1.375 ± 0.122), while LNRT2 and LNRT2/T1 (LNRT2: 1.389 ± 0.086, LNRT2/T1: 2.511 ± 0.295) were significantly lower than those of HGG (LNRT2: 1.527 ± 0.191, LNRT2/T1: 3.263 ± 0.657), and BM (LNRT2: 1.504 ± 0.089, LNRT2/T1: 3.103 ± 0.830). There was no significant difference in CER among the three groups ($P > .05$). ROC curve analysis of LNRT1, LNRT2, LNRT1CE, and LNRT2/T1 could be used to discriminate PCNSL from HGG and BM, with LNRT1CE having the largest area under the curve of 0.873, sensitivity of 0.963 and specificity of 0.669.

Conclusion • MRI lesion morphological features and signal intensity ratio are important for discriminating HGG from PCNSL and BM. As a quantitative parameter, tumor signal intensity ratio can provide an important supplement for subjective judgment, to improve the accuracy of tumor qualitative diagnosis and differential diagnosis. (*Altern Ther Health Med.* 2023;29(8):816-821).

Hongmei Yu, MM; Min Chen, MM; Yi Huang, BM; Peng Wang, MM; Jianhao Li, MM; Qing Li, BM; Rui Jiang, MM; Department of Radiology, The General Hospital of Western Theater Command, Chengdu, China.

Corresponding author: Rui Jiang, MM
E-mail: jiangrui07@sina.com

INTRODUCTION

Glioma is a neuroepithelial tissue-derived tumor with morphological characteristics of astrocytes, oligodendrocytes, ependymal cells, or choroidal plexus cells. It is the most common primary malignant tumor of the central nervous system in adults. According to the 2016 WHO grading standards, it is divided into low-grade gliomas (LGG; WHO grades I and II) and high-grade gliomas (HGG; WHO grades III and IV) based on the degree of malignancy. HGG has a high degree of malignancy, rapid progression, and poor prognosis, and is clinically treated with surgery combined with radiotherapy and chemotherapy.[1,2] PCNSL is mostly of B cell origin, closely related to immune function, with a low incidence rate and unknown pathogenesis. The clinical treatment is mainly chemotherapy and/or radiotherapy.[3] Brain metastases are one of the most common adult intracranial malignant tumors. The most common origin sites of brain metastases are lung cancer, breast cancer, and melanoma, and they only present as single-brain metastases

with central nervous system symptoms or isolated intracranial lesions. Surgery, targeted therapy, conformal radiotherapy, or chemotherapy are usually used for comprehensive treatment.[4] How to effectively distinguish HGG, PCNSL, and BM before surgery is of great significance for the selection of clinical treatment plans and prognosis.

MRI is an important examination tool for the diagnosis of intracranial tumors, and in most cases, physicians can make the diagnosis and differential diagnosis based on the main imaging manifestations of the lesion, HGG mostly showed intracranial necrocysts, uneven or cyclic enhancement, while PCNSL mainly showed a mass with obvious homogeneity enhancement. BM showed various imaging manifestations, which were related to the primary tumor type. In clinical work, there were many tumors with atypical or similar imaging manifestations, which were difficult to identify and easy to be misdiagnosed by doctors' experience and senior-related imaging, thus affecting the choice of the best clinical treatment plan and patient prognosis.[5-7] In recent years, MRI multimodal imaging and image-omics and other advanced technologies have made great progress in the diagnosis and differential diagnosis of brain tumors, such as DWI, DTI, MRS, PWI, ASL, and other advanced sequences or the use of image-omics methods can greatly improve the accuracy of qualitative diagnosis of intracranial tumors[8-12] but they require more time and increase patient costs, and the inconsistency of equipment and parameters is such that there is a lack of uniform thresholds for differential diagnosis. The use of conventional MRI morphological manifestations and its quantitative parameters for differential diagnosis of tumors has rarely been reported. In this study, we determined whether the morphological characteristics of HGG, PCNSL, and BM tumors and measured the lesiontonormal parenchymaratio (LNR) signal ratio of the lesion to determine whether it can be used as a quantitative parameter for the differential diagnosis of the three, providing an important supplement to the subjective analysis.

MATERIALS AND METHODS

Retrospective analysis of patients with pathologically diagnosed high-grade glioma, primary central nervous system lymphoma, and solitary brain metastases at The General Hospital of Western Theater Command between August 2014 and December 2021. Inclusion criteria, 1) all patients obtained pathological diagnosis by surgery or biopsy; 2) no history of relevant treatment (such as biopsy, radiotherapy, chemotherapy, and glucocorticoid treatment) before MRI examination; 3) complete MRI examination data (basic sequence of T1WI, T2WI and enhanced T1WI) with good image quality; 4) all patients with normal immune function. Exclusion criteria, 1) incomplete MRI data or poor image quality; 2) systemic lymphoma with intracranial metastases; 3) patients with previous cranial surgery, epilepsy, or stroke; 4) combined with other tumors. This retrospective study was approved by the ethics committee and exempted from patient informed consent requirements. A total of 154 patients were included according to inclusion and exclusion criteria, including 92 HGG cases of HGG (57 males and 35 females, mean age 51.9 ± 14.5), 27 cases of PCNSL (21 males and 6 females, mean age 53 ± 12.8), and 35 cases of BM (22 males and 13 females, mean age 57.8 ± 10.4), The primary foci originated from the lung in 24 cases, from the gastrointestinal tract in 5 cases, from the breast in 3 cases, from the uterus in 2 cases, and from the mediastinum in 1 case. The main clinical symptoms were headache and dizziness, some of which were accompanied by nausea, vomiting, epilepsy, visual disturbance, mental abnormalities, or hemiparesis of the limbs.

MRI examination methods

All 154 patients underwent plain and enhanced cranial MRI scans. Using a Philips 3.0T superconducting MR scanner or GE SIGNA pioneer 3.0T MR scanner, with a 16-channel head and neck orthogonal coil, all patients underwent axial flat-scan T_1WI (TR 2000 ms/1750 ms, TE 20 ms/20 ms), T_2WI (TR 2000 ms/4376 ms, TE 85 ms/105ms). and the enhancing contrast agent was gadolinium penate glucosamine injection at Coronal, sagittal and axial T_1WI lipid-suppressed enhancement scans (TR 188 m/s/175ms, TE 5 m/s/5ms) were performed at a flow rate of 0.1 mmol/kg and 3.0 ml/s by intravenous push in the forearm with a layer thickness of 6 mm and a layer spacing of 1 mm, FOV 23 cm × 23 cm.

Image Analysis and Data Measurement

Two senior neurological doctors from the Department of Radiology will review the films independently, and in case of disagreement, a unified conclusion will be reached through consultation. The main qualitative imaging parameters to be observed include tumor site, morphology, intratumoral hemorrhage, necrotic cystic lesions, degree of peripheral edema, and enhancement pattern. The tumor site was classified as supratentorial and sub-tentorial, and the enhancement pattern was classified as uniform enhancement, inhomogeneous enhancement, and wreath-like enhancement, and the degree of peritumor edema: (a) No edema; (b) Mild: the extent of edema is less than 1/2 of the maximum diameter of the tumor; (c) Moderate: the extent of edema is between 1/2 of the maximum diameter of the tumor and the maximum diameter; (d) Severe: the extent of edema exceeds the maximum diameter of the tumor. Data measurement: (a) tumor diameter, the maximum tumor diameter was measured on axial T1WI-enhanced images; (b) the signal value of the lesion was measured on axial T1WI, T2WI, and T1WI lipid-suppressed-enhanced images with the signal intensity (SI) of the lateral brain parenchyma on the same level,[13] and each measurement tried to avoid vascular, hemorrhagic and cystic necrosis areas, and the largest level of the lesion was selected for measurement, and the ROI was selected for 20-40 mm^2 measurement three times, and the average value was taken. The lesion/contralateral normal brain parenchymal signal

ratio (LNR) and contrast enhancement ratio (CER) were calculated, LNR=SI lesion/SI normal brain parenchyma, CER= (SI enhancement-SI panning)/SI panning, LNRT2/T1=LNRT2/LNRT1.

Statistical Methods

SPSS version 24.0 software was applied for statistical analysis of the data. The Kolmogorov-Smirnov test was used to test whether the measures conformed to a normal distribution, and those with a normal distribution were expressed as $\bar{x} \pm s$. Comparison of HGG, PCNSL, and BM LNRT1, LNRT2, LNRT1CE, CER, LNRT2/T1 by One-way analysis of variance (ANOVA), followed by a two-group comparison using the post hoc Tamhane test, applying subject operating characteristic (ROC) curves to evaluate the diagnostic efficacy of the measured parameters and calculating the optimal threshold for differential diagnosis and its sensitivity and specificity; the count data were expressed as number of cases and compared using the χ^2 test or Fisher's exact test; $P < .05$ was considered a statistically significant difference.

RESULTS

Comparison of HGG, PCNSL, and BM imaging classification variables

HGG, PCNSL, and BM all occurred mostly in the supratentorial area, and there was no statistically significant difference in the site of tumorigenesis (supratentorial/intratentorial) among the three ($P > .05$). HGG mainly shows irregular morphology, intra-tumor hemorrhage, necrotic cystic lesions, moderate-to-severe peritumor edema, enhancement is mostly heterogeneous, and wreath-like intensification; PCNSL mainly shows irregular morphology, rare intra-tumor hemorrhage and necrotic cystic lesions, varying degrees of edema, and enhancement is mainly obvious uniform or inhomogeneous enhancement; BM mainly shows regular or irregular morphology, with less intra-tumor hemorrhage and necrotic cysts than HGG, and moderate to severe peritumor edema. The differences in tumor morphology, peritumoral edema, intratumoral hemorrhage, necrotic cystic degeneration, and enhancement patterns between HGG, PCNSL, and BM were statistically significant ($P < .05$). See Table 1.

Table 1. Statistics of HGG, PCNSL, and BM MRI categorical variables n(%)

Parameters	HGG (n=92)	PCNSL (n = 27)	BM (n = 35)	χ^2	*P* value
Tumor site					
Curtain Up	83 (90.2)	23 (85.2)	30 (85.7)	1.095	.600
Under the Curtain	9 (9.8)	4 (14.8)	5 (14.3)		
Tumor morphology					
Rules	21 (22.8)	8 (29.6)	18 (51.4)	9.794	.007
	71 (77.2)	19 (70.4)	17 (48.6)		
Peritumoral edema					
None	0 (0)	2 (7.4)	4 (11.4)	29.771	<.001
Mild	5 (5.4)	10 (37.0)	4 (11.4)		
Moderate	32 (34.8)	9 (33.3)	11 (31.4)		
Severe	55 (59.8)	6 (22.2)	16 (45.7)		
Intratumoral hemorrhage					
None	55 (59.8)	23 (85.2)	30 (85.7)	11.682	.003
All	37 (40.2)	4 (14.8)	5 (14.3)		
necrotic cystic degeneration					
None	12 (13.0)	21 (77.8)	21 (60.0)	50.785	<.001
All	80 (87.0)	6 (22.2)	14 (40.0)		
Reinforcement method					
Homogeneous reinforcement	2 (2.2)	19 (70.4)	12 (34.3)	62.933	<.001
Uneven reinforcement	58 (63.0)	6 (22.2)	17 (48.6)		
Wreath-like reinforcement	32 (34.8)	2 (7.4)	6 (17.1)		

Abbreviations: HGG, high-grade glioma; PCNSL, primary central nervous system lymphoma; BM, brain metastases.

Table 2. One-way ANOVA for HGG, PCNSL, and BM MRI continuous variables

Parameter	HGG (n = 92)	PCNSL (n = 27)	BM (n=35)	*P* value (ANOVA)
LNRT1	0.480 ± 0.077	0.558 ± 0.050	0.514 ± 0.120	<.001
LNRT2	1.527 ± 0.191	1.389 ± 0.086	1.504 ± 0.089	.001
LNRT1CE	1.425 ± 0.160	1.637 ± 0.125	1.375 ± 0.122	<.001
CER	1.435 ± 0.421	1.437 ± 0.367	1.429 ± 0.517	.997
LNRT2/T1	3.263 ± 0.657	2.511 ± 0.295	3.103 ± 0.830	<.001
Pairwise comparison with post hoc Tamhane test–*P* values				
Parameter	HGG vs PCNSL	HGG vs BM	PCNSL vs BM	
LNRT1	<.001	.321	.154	
LNRT2	<.001	.732	<.001	
LNRT1CE	<.001	.086	<.001	
CER	.985	.941	.942	
LNRT2/T1	<.001	.674	.001	

Abbreviations: HGG, high-grade glioma; PCNSL, primary central nervous system lymphoma; BM, brain metastases.

Table 3. Differential diagnostic ability of quantitative signal percentage parameters for PCNSL with HGG and BM

Parameter	Truncated values	AUC(95% CI)	Sensitivity (%)	Specificity (%)	*P* value
LNRT1	0.505	0.751 (0.671-0.830)	88.9	58.3	<.001
LNRT2	1.463	0.748 (0.667-0.829)	85.2	63.8	<.001
LNRT1CE	1.469	0.873 (0.816-0.931)	96.3	66.9	<.001
LNRT2/T1	2.830	0.825 (0.756-0.895)	88.9	71.7	<.001

Abbreviations: AUC, area under the curve; CI, confidence interval; HGG, high-grade glioma; PCNSL, primary central nervous system lymphoma; BM, brain metastases.

Comparison of quantitative parameters of HGG, PCNSL, and BM imaging and ROC curve analysis

The quantitative parameters of HGG, PCNSL, and BM signal intensity percentages are shown in Table 3, and the differences of LNRT1, LNRT2, LNRT1CE, and LNRT2/T1 among HGG, PCNSL, and BM were statistically significant by one-way ANOVA ($P < .001$), and there was no statistical difference between the three CER groups ($P > .05$), with post hoc Tamhane test for comparison between groups showed that PCNSL, LNRT1, and LNRT1CE (LNRT1: 0.558 ± 0.050, LNRT1CE: 1.637 ± 0.125) were significantly higher than HGG (LNRT1: 0.480 ± 0.077, LNRT1CE: 1.425 ± 0.160), and BM (LNRT1: 0.514 ± 0.120, LNRT1CE: 1.375 ± 0.122), while LNRT2 and LNRT2/T1 (LNRT2: 1.389 ± 0.086, LNRT2/T1: 2.511 ± 0.295) were significantly lower than HGG (LNRT2: 1.527 ± 0.191, LNRT2/T1: 3.263 ± 0.657), and BM (LNRT2: 1.504 ± 0.089, LNRT2/T1: 3.103 ± 0.830), and the differences were statistically significant ($P < .001$), and the differences between HGG and BM groups were not statistically significant ($P > .05$). ROC curve analysis showed that the cut-off values for LNRT1, LNRT2, LNRT1CE and LNRT2/T1 to discriminate PCNSL from non-PCNSL (HGG and BM) were approximately 0.505, 1.463, 1.469 and 2.830, respectively, with LNRT1CE having the largest area under the curve at 0.873, sensitivity 0.963 and specificity 0.669, see Tables 2 and 3, Figures 1-3, Figures 4 and 5.

Figure 1A-C. Male, 53 years old, HGG, right basal ganglia area and temporal lobe mass-like occupancy with slightly high signal on T_2WI and low signal on T_1WI, heterogeneous enhancement with wreath-like enhancement at the edges, quantitative parameters LNRT1, LNRT2, LNRT1CE, CER, and LNRT2/T1 were 0.603, 1.825, 1.573,1.332 and 3.028.

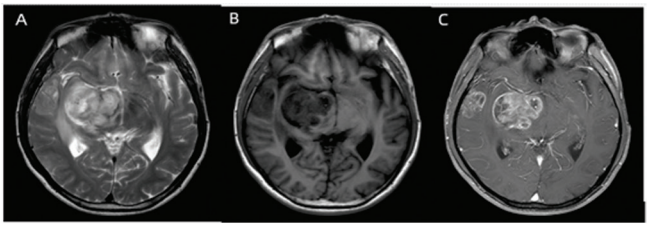

Figure 2A-C. Female, 51 years old, PCNSL, irregular mass-like occupancy in the right occipital lobe with high signal in T_2WI and slightly low signal in T_1WI, uneven enhancement after enhancement, with cystic necrotic areas seen within, quantitative parameters LNRT1, LNRT2, LNRT1CE, CER and LNRT2/T1 were 0.604, 1.399, 1.522,1.608, and 2.317.

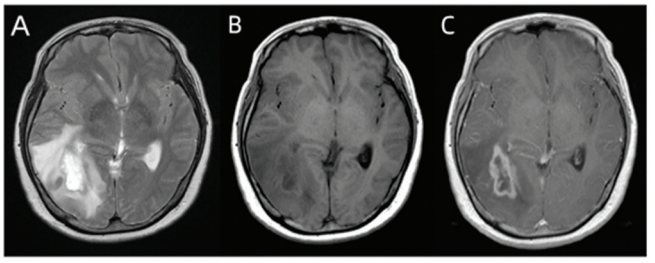

Figure 3A-C. Female, 45 years old, brain metastasis from lung cancer, left frontal lobe occupancy with peripheral severe edema, slightly high signal on T_2WI, slightly low signal on T_1WI, inhomogeneous enhancement with cystic necrotic areas seen within, quantitative parameters LNRT1, LNRT2, LNRT1CE, CER, and LNRT2/T1 were 0.509, 1.549, 1.557 1.794 and 3.042.

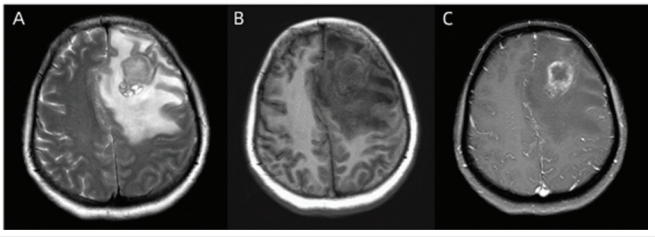

Figure 4. ROC curves of LNRT1 and LNRT1CE to discriminate PCNSL from HGG and BM (Blue lines: LNRT1, Green lines: LNRT1CE, Yellow lines: Guide line)

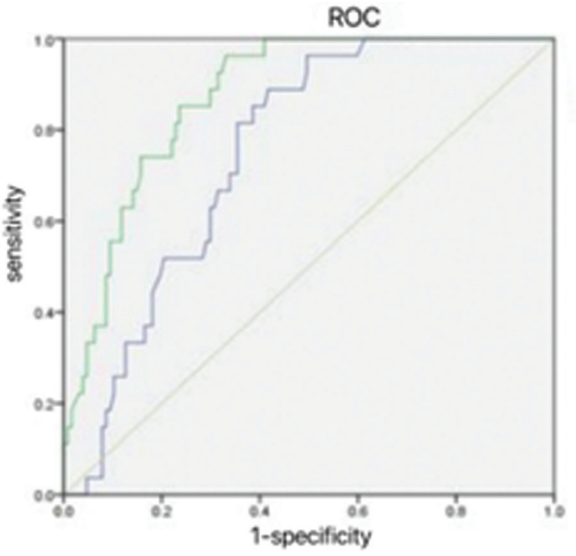

Figure 5. ROC curves of LNRT2 and LNRT2T1 to discriminate PCNSL from HGG and BM (Blue lines: LNRT2, Green lines: LNRT2T1, Yellow lines: Guide line)

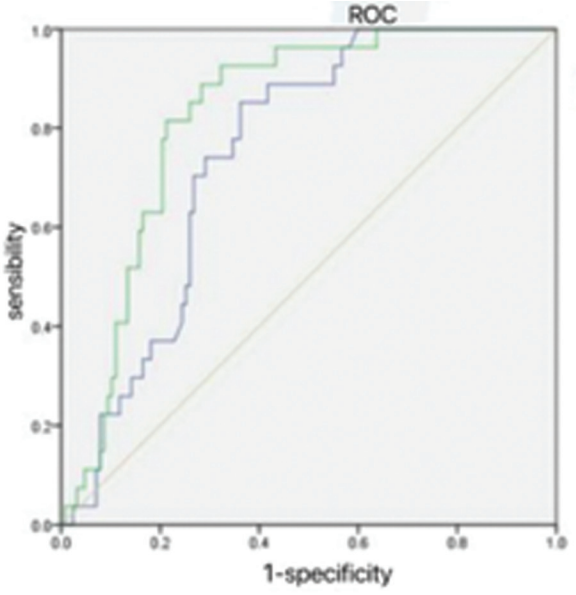

DISCUSSION

Comparison of morphological characteristics of HGG, PCNSL, and BM

By preliminary observation of the morphological characteristics and intensification pattern of the tumor, HGG showed mostly irregular morphology, mostly heterogeneous and/or wreath-like intensification (63%, 34.8%) with obvious intra-tumor necrotic cystic changes (87%) and moderate to severe peritumor edema (34.8%, 59.8%), while 70.4% of PCNSL cases showed obvious homogeneity, only 14.3% showed hemorrhage and 40% showed necrotic cystic changes. BM mainly showed uniform or heterogeneous enhancement (34.3%, 48.6%), with less intra-tumor hemorrhage and necrotic cystic lesions than HGG.HGG, PCNSL, and BM have significant differences in tumor morphology, peritumor edema, intratumor hemorrhage, necrotic cystic changes, and comparison of enhancement patterns, which is consistent with most previous studies.[14-16] The inconsistency in morphological characteristics and enhancement patterns of the three types of tumors was analyzed to be closely related to the pathophysiology of the tumors. The highly aggressive growth of HGG with variable rates in all directions showed irregular morphology on imaging, extensive irregular microvascular proliferation within the lesions, varying

degrees of disruption of the blood-brain barrier and increased permeability, resulting in tumors with markedly heterogeneous enhancement, multiple immature vascular networks and increased oxygen metabolic rate within the lesions increased, causing significant tumor necrocystic degeneration.[17,18] Most PCSNL are B-cell lymphomas with dense cellular tissue, often growing infiltrative around the perivascular space and encircling blood vessels, disrupting the blood-brain barrier, with enhancement mostly showing marked uniform enhancement, and mixed brain edema caused by mainly vascular-derived edema plus tumor cell infiltration and microvascular proliferation in HGG and PCSNL.[19] The BM mostly shows expansive growth with pressure displacement of the surrounding brain tissue, without signs of brain parenchymal infiltration, and the blood supply is mostly rich.

Comparative analysis of HGG, PCNSL, and BM signal intensity ratio differences

This study, by quantitative analysis of the differences in signal intensity ratios of HGG, PCNSL, and BM. PCNSL LNRT1 and LNRT1CE were significantly higher than HGG and BM, while LNRT2 and LNRT2/T1 were significantly lower than HGG and BM, HGG LNRT1 was lower than BM, and LNET2, LNRT1CE, CER, and LNRT2/T1 were higher than BM, but there was no statistical difference between the two. ROC curve analysis to identify PCNSL and non-PCNSL (HGG and BM), where LNRT1CE had the largest area under the curve of 0.873, sensitivity of 0.963, and specificity of 0.669, which is consistent with the findings of Han Y,[13] but Han Y et al. concluded that LNRT2/T1 was the best parameter to identify PCNSL from glioblastoma, the author believes that it may be related to the inconsistency of study population, sample size, tumor type and ROI selection. The difference in signal intensity ratio between HGG and PCSNL and BM can objectively reflect the difference in pathophysiology and microenvironment of the three.[13,20] PCNSL contains a large number of tumor cells and reticulocytes, and the large nucleoplasmic ratio leads to the lower water content of the tumor. Its internal necrotic cystic lesions are rare, while the tumor grows along the perivascular area and disrupts the blood-brain barrier, leading to shortened T1 and T2*, showing significant uniform enhancement and quantitative imaging parameters BM histopathology is related to the type of primary tumor and its imaging performance is relatively complex, and some studies[19-22] concluded that neither tumor ADC nor rCBV can be used as effective indicators to distinguish BM from HGG. The present study also showed that there was no difference in LNR between the two groups.

The advantages of this study in the differential diagnosis of intracranial tumors

Most previous studies have investigated MRI advanced sequences and imaging histology for the differential diagnosis of HGG, PCNSL, and BM.[6,21,23-25] In this study, we quantified the differences between the three by conventional MRI LNR, whose main advantages are: (i) conventional MRI imaging sequences for intracranial tumors include T1WI, T2WI, and T1WICE, which have fast scan time, relatively low cost and Most of the literature[8,17,26,27] reported that T1WICE is the preferred sequence for diagnosis and differential diagnosis of brain tumors; (ii) although the tumor morphological features, enhancement patterns, and signal differences can be observed by the naked eye for preliminary judgment of tumor nature, they are affected by various factors such as physician qualifications, differences in MRI sequence parameters and atypical tumor features; (iii) The author used LNR as a quantitative parameter, and the data obtained were objective, reliable, and reproducible. It was not affected by different MRI devices or sequence parameters. The conventional MRI sequence was used to observe the morphological characteristics of lesions subjectively and measure the number of LNR for objective evaluation and comparison, which was simple and fast and could improve the accuracy of tumor qualitative diagnosis. Studies by many scholars[28-30] have shown that LNR is important in the differential diagnosis of tumors, and LNRT2/T1 has achieved good results in the differential diagnosis of glioblastoma, brain demyelinating lesions, and benign and malignant lesions of the breast.

The present study also has some shortcomings: (i) the sample sizes of PCSNL and BM were relatively small, and BM was not analyzed by type of primary tumor individually; (ii) only conventional MRI sequences were analyzed, and advanced MRI sequences and imaging histology were not studied.

CONCLUSION

Based on the morphological characteristics of the tumor and the LNR, it is important for the differential diagnosis of PCSNL from HGG and BM. For cases with atypical or complex imaging manifestations, LNR can serve as a quantitative parameter to provide an important supplement for subjective analysis, thereby improving the qualitative and differential diagnosis capabilities of tumors.

REFERENCES

1. Watts C. Surgical management of high-grade glioma: a standard of care. *CNS Oncol*. 2012;1(2):181-192. doi:10.2217/cns.12.26
2. Luo C, Xu S, Dai G, Xiao Z, Chen L, Liu Z. Tumor treating fields for high-grade gliomas. *Biomed Pharmacother*. 2020;127:110193. doi:10.1016/j.biopha.2020.110193
3. Calimeri T, Steffanoni S, Gagliardi F, Chiara A, Ferreri AJM. How we treat primary central nervous system lymphoma. *ESMO Open*. 2021;6(4):100213. doi:10.1016/j.esmoop.2021.100213
4. Suh JH, Kotecha R, Chao ST, Ahluwalia MS, Sahgal A, Chang EL. Current approaches to the management of brain metastases. *Nat Rev Clin Oncol*. 2020;17(5):279-299. doi:10.1038/s41571-019-0320-3
5. Lin X, Khan IRA, Seet YHC, Lee HY, Yu WY. Atypical radiological findings of primary central nervous system lymphoma. *Neuroradiology*. 2020;62(6):669-676. doi:10.1007/s00234-020-02377-0
6. Suh HB, Choi YS, Bae S, et al. Primary central nervous system lymphoma and atypical glioblastoma: differentiation using radiomics approach. *Eur Radiol*. 2018;28(9):3832-3839. doi:10.1007/s00330-018-5368-4
7. Choi YS, Lee HJ, Ahn SS, et al. Primary central nervous system lymphoma and atypical glioblastoma: differentiation using the initial area under the curve derived from dynamic contrast-enhanced MR and the apparent diffusion coefficient. *Eur Radiol*. 2017;27(4):1344-1351. doi:10.1007/s00330-016-4484-2
8. Bathla G, Priya S, Liu Y, et al. Radiomics-based differentiation between glioblastoma and primary central nervous system lymphoma: a comparison of diagnostic performance across different MRI sequences and machine learning techniques. *Eur Radiol*. 2021;31(11):8703-8713. doi:10.1007/s00330-021-07845-6
9. Xia W, Hu B, Li H, et al. Deep Learning for Automatic Differential Diagnosis of Primary Central Nervous System Lymphoma and Glioblastoma: Multi-Parametric Magnetic Resonance Imaging Based Convolutional Neural Network Model. *J Magn Reson Imaging*. 2021;54(3):880-887. doi:10.1002/jmri.27592
10. Pennig L, Hoyer UCI, Goertz L, et al. Primary Central Nervous System Lymphoma: Clinical Evaluation of Automated Segmentation on Multiparametric MRI Using Deep Learning. *J Magn Reson Imaging*. 2021;53(1):259-268. doi:10.1002/jmri.27288

11. Heynold E, Zimmermann M, Hore N, et al. Physiological MRI Biomarkers in the Differentiation Between Glioblastomas and Solitary Brain Metastases. *Mol Imaging Biol*. 2021;23(5):787-795. doi:10.1007/s11307-021-01604-1
12. Cindil E, Şendur HN, Cerit MN, et al. Validation of combined use of DWI and percentage signal recovery-optimized protocol of DSC-MRI in differentiation of high-grade glioma, metastasis, and lymphoma. *Neuroradiology*. 2021;63(3):331-342. doi:10.1007/s00234-020-02522-9
13. Han Y, Wang ZJ, Li WH, et al. Differentiation Between Primary Central Nervous System Lymphoma and Atypical Glioblastoma Based on MRI Morphological Feature and Signal Intensity Ratio: A Retrospective Multicenter Study. *Front Oncol*. 2022;12:811197. doi:10.3389/fonc.2022.811197
14. Malikova H, Koubska E, Weichet J, et al. Can morphological MRI differentiate between primary central nervous system lymphoma and glioblastoma? *Cancer Imaging*. 2016;16(1):40. doi:10.1186/s40644-016-0098-9
15. Ko CC, Tai MH, Li CF, et al. Differentiation between Glioblastoma Multiforme and Primary Cerebral Lymphoma: Additional Benefits of Quantitative Diffusion-Weighted MR Imaging. Sherman JH, ed. *PLOS ONE*. 2016;11(9):e0162565. doi:10.1371/journal.pone.0162565.
16. Chen Y, Zhan A. Clinical value of magnetic resonance imaging in identifying multiple cerebral gliomas from primary central nervous system lymphoma. *Oncol Lett*. 2019;18(1):593-598. doi:10.3892/ol.2019.10352
17. Wang P, Shi YH, Li JY, Zhang CZ. Differentiating Glioblastoma from Primary Central Nervous System Lymphoma: The Value of Shaping and Nonenhancing Peritumoral Hyperintense Gyral Lesion on FLAIR Imaging. *World Neurosurg*. 2021;149:e696-e704. doi:10.1016/j.wneu.2021.01.114
18. Wu W, Deng Z, Alafate W, et al. Preoperative Prediction Nomogram Based on Integrated Profiling for Glioblastoma Multiforme in Glioma Patients. *Front Oncol*. 2020;10:1750. doi:10.3389/fonc.2020.01750
19. Neska-Matuszewska M, Bladowska J, Sąsiadek M, Zimny A. Differentiation of Glioblastoma multiforme, Metastases and Primary Central Nervous System Lymphomas Using Multiparametric Perfusion and Diffusion MR Imaging of a Tumor Core and a Peritumoral zone—Searching for a Practical Approach. Fillmore H, ed. *PLOS ONE*. 2018;13(1):e0191341. doi:10.1371/journal.pone.0191341.
20. Anwar SSM, Baig MZ, Laghari AA, et al. Accuracy of apparent diffusion coefficients and enhancement ratios on magnetic resonance imaging in differentiating primary cerebral lymphomas from glioblastoma. *Neuroradiol J*. 2019;32(5):328-334. doi:10.1177/1971400919857556
21. Lee MD, Baird GL, Bell LC, Quarles CC, Boxerman JL. Utility of Percentage Signal Recovery and Baseline Signal in DSC-MRI Optimized for Relative CBV Measurement for Differentiating Glioblastoma, Lymphoma, Metastasis, and Meningioma. *AJNR Am J Neuroradiol*. 2019;40(9):1445-1450. doi:10.3174/ajnr.A6153
22. Beig Zali S, Alinezhad F, Ranjkesh M, Daghighi MH, Poureisa M. Accuracy of apparent diffusion coefficient in differentiation of glioblastoma from metastasis. *Neuroradiol J*. 2021;34(3):205-212. doi:10.1177/1971400920983678
23. He YX, Qu CX, He YY, Shao J, Gao Q. Conventional MR and DW imaging findings of cerebellar primary CNS lymphoma: comparison with high-grade glioma. *Sci Rep*. 2020;10(1):10007. doi:10.1038/s41598-020-67080-9
24. Kickingereder P, Wiestler B, Sahm F, et al. Primary central nervous system lymphoma and atypical glioblastoma: multiparametric differentiation by using diffusion-, perfusion-, and susceptibility-weighted MR imaging. *Radiology*. 2014;272(3):843-850. doi:10.1148/radiol.14132740
25. Wang S, Kim S, Chawla S, et al. Differentiation between glioblastomas, solitary brain metastases, and primary cerebral lymphomas using diffusion tensor and dynamic susceptibility contrast-enhanced MR imaging. *AJNR Am J Neuroradiol*. 2011;32(3):507-514. doi:10.3174/ajnr.A2333
26. Xia W, Hu B, Li H, et al. Multiparametric-MRI-Based Radiomics Model for Differentiating Primary Central Nervous System Lymphoma From Glioblastoma: Development and Cross-Vendor Validation. *J Magn Reson Imaging*. 2021;53(1):242-250. doi:10.1002/jmri.27344
27. Wang Q, Li Q, Mi R, et al. Radiomics Nomogram Building From Multiparametric MRI to Predict Grade in Patients With Glioma: A Cohort Study. *J Magn Reson Imaging*. 2019;49(3):825-833. doi:10.1002/jmri.26265
28. Yamamoto S, Sanada T, Sakai M, et al. Prediction and Visualization of Non-Enhancing Tumor in Glioblastoma via T1w/T2w-Ratio Map. *Brain Sci*. 2022;12(1):99-99. doi:10.3390/brainsci12010099
29. Nakamura K, Chen JT, Ontaneda D, Fox RJ, Trapp BD. T1-/T2-weighted ratio differs in demyelinated cortex in multiple sclerosis. *Ann Neurol*. 2017;82(4):635-639. doi:10.1002/ana.25019
30. Malikova MA, Tkacz JN, Slanetz PJ, Guo CY, Aakil A, Jara H. Evaluation of T1/T2 ratios in a pilot study as a potential biomarker of biopsy: proven benign and malignant breast lesions in correlation with histopathological disease stage. *Future Sci OA*. 2017;3(3):FSO197-FSO197. doi:10.4155/fsoa-2016-0063